ACS APPLIED MATERIALS & INTERFACES

Research Article

www.acsami.org

Selective Sintering of Metal Nanoparticle Ink for Maskless Fabrication of an Electrode Micropattern Using a Spatially Modulated Laser Beam by a Digital Micromirror Device

Kunsik An,[†,¶] Sukjoon Hong,[‡,¶] Seungyong Han,[†] Hyungman Lee,[†,§] Junyeob Yeo,*[,‡] and Seung Hwan Ko*[,‡]

[†]Department of Mechanical Engineering, KAIST, 291 Daehak-ro, Yuseong-Gu, Daejeon 305-701, Korea

[‡]Applied Nano and Thermal Science Lab, Department of Mechanical Engineering, Seoul National University, 1 Gwanak-ro, Gwanak-gu, Seoul 151-742, Korea

[§]Nano sensors and device team, Korea electronics technology institute (KETI), Seongnam-si, Gyeonggi-do 463-816, Korea

ABSTRACT: We demonstrate selective laser sintering of silver (Ag) nanoparticle (NP) ink using a digital micromirror device (DMD) for the facile fabrication of 2D electrode pattern without any conventional lithographic means or scanning procedure. An arbitrary 2D pattern at the lateral size of 25 μm × 25 μm with 160 nm height is readily produced on a glass substrate by a short exposure of 532 nm Nd:YAG continuous wave laser. The resultant metal pattern exhibits low electrical resistivity of 10.8 uΩ · cm and also shows a fine edge sharpness by the virtue of low thermal conductivity of Ag NP ink. Furthermore, 10 × 10 star-shaped micropattern arrays are fabricated through a step-and-repeat scheme to ensure the potential of this process for the large-area metal pattern fabrication.

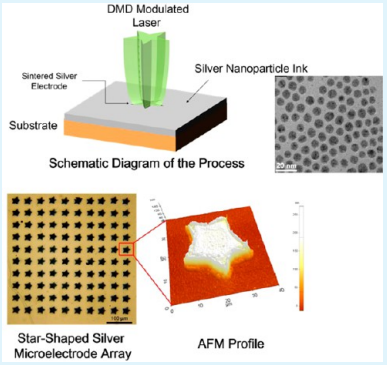

KEYWORDS: *digital micromirror device, nanoparticle ink, nanoparticle laser sintering, nonvacuum environment, low temperature metal thin film patterning*

1. INTRODUCTION

In various electronic devices, thin film electrode is an inevitable component[1−3] and the conventional photolithography process together with vacuum metal deposition has been long used to fabricate a patterned electrode layer. Despite great success, the conventional metal patterning process suffers from numerous problems including high-priced vacuum conditions, high temperature environment, toxic chemicals, and multiple steps which increase the cost and complexity of the overall process. To overcome these problems, a number of alternative metal patterning techniques have been developed, and the sintering of metal nanoparticles (NPs) has attracted wide attention among these techniques to acquire an electrode layer[4−6] without any harsh environments or expensive equipment.

For the general metal NP sintering process, metal NP ink is first printed on a substrate at a desired pattern by various printing techniques such as inkjet printing,[7] gravure printing,[8] screen printing,[9] and nanoimprinting[10] followed by an annealing process in a hot furnace for a certain time to transform individual NPs into a continuous conducting film. This process is much simpler compared to the conventional photolithography process, but the resultant metal pattern generally exhibits limited resolution and the annealing process often requires considerable time and temperature.

Recently, laser sintering of metal NP ink has been reported to solve these drawbacks.[11−13] In a typical experiment, metal NP ink is coated on a substrate first and a focused laser, as a localized heat source, is scanned at an arbitrary pattern to conduct patterning and annealing of metal NP ink in a single step. Due to the small size of a focused laser spot and low thermal conductivity of metal NP ink, the minimum feature size of the laser sintered metal pattern easily reaches micrometer scale, while the area subject to the laser sintering can be extended to several centimeters by using a galvanomirror and telecentric lens. However, laser scanning is only suitable for the fabrication of line patterns. For an arbitrary 2D patterning, the laser spot has to go through a raster scanning at a fixed hatch size, which can be very time-consuming for a dense pattern in particular.

In this study, 2D laser sintering of metal NP ink at an arbitrary pattern is achieved without any scanning procedure by using a digital micromirror device (DMD). Since each micromirror in DMD can be controlled separately using digital signal, DMD has been widely applied to maskless lithography[14−17] to pattern the photoresist layer. Instead, we utilize

Received: November 24, 2013
Accepted: January 28, 2014
Published: January 28, 2014

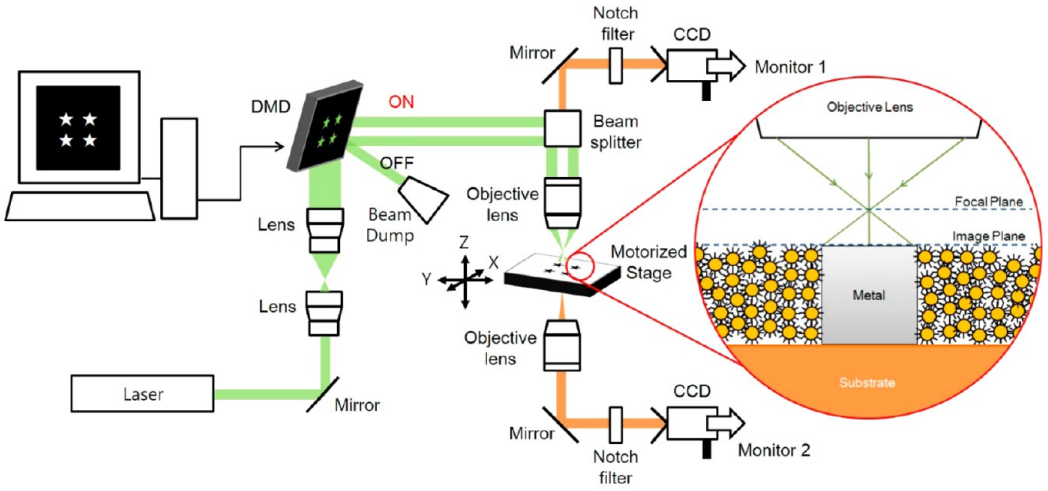

Figure 1. Schematic illustration of the optical system for Ag NP sintering by a DMD modulated laser beam.

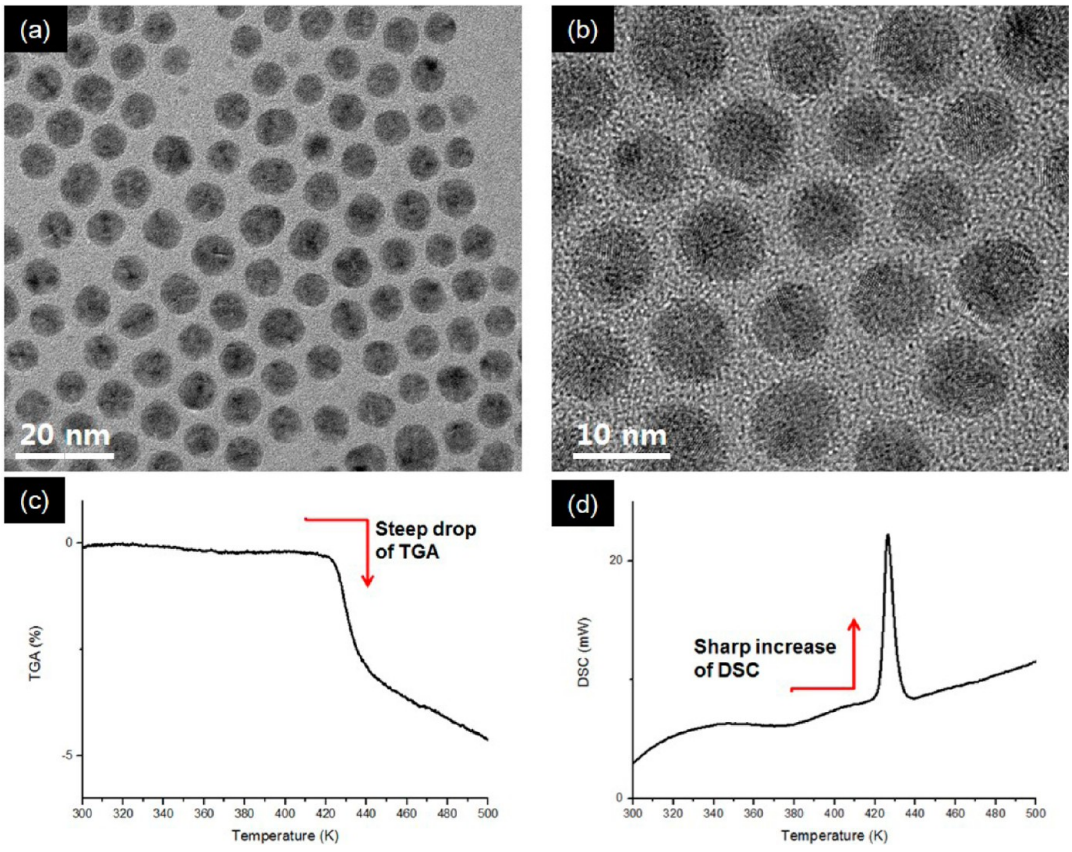

Figure 2. (a, b) Transmission electron microscopic images of the Ag nanoparticles with self-assembled monolayer. (c) Thermogravimetric analysis profile. (d) Differential scanning calorimetric profile.

DMD for direct 2D sintering of metal NP ink through direct imaging of DMD pattern on the silver (Ag) NP ink. By focusing DMD modified laser beam on the Ag NP ink, 2D sintering of Ag NP ink with fine edge sharpness and low electrical resistivity is readily achieved with a single exposure. The Ag NPs used for the sintering is characterized by thermogravimetric analysis (TGA), differential scanning calorimetry (DSC), and transmission electron microscopy (TEM), while the temperature generated by DMD modified laser beam is estimated by finite element (FE) calculation to analyze the sintering condition. Furthermore, by fabricating the Ag micropattern array through a step-and-repeat scheme, we confirm that this process has a potential for large-area high-resolution metal patterning.

2. EXPERIMENTAL SECTION

Ag NPs are prepared from a two-phase reduction method with subtle modification which was reported from Kogel et al.[18] 0.2 M tetroacylammonium bromide ($(C_8H_{17})_4NBr$) is added in 20.4 mL of toluene. Pure water with 30 mM silver nitride is added to the toluene-based solution. After vigorous stirring for 1 h, silver ions are transferred to the organic solution from aqueous solution. Aqueous solution is removed, and 0.16 mg of dodecanethiol is added with

dx.doi.org/10.1021/am405323c | ACS Appl. Mater. Interfaces 2014, 6, 2786−2790

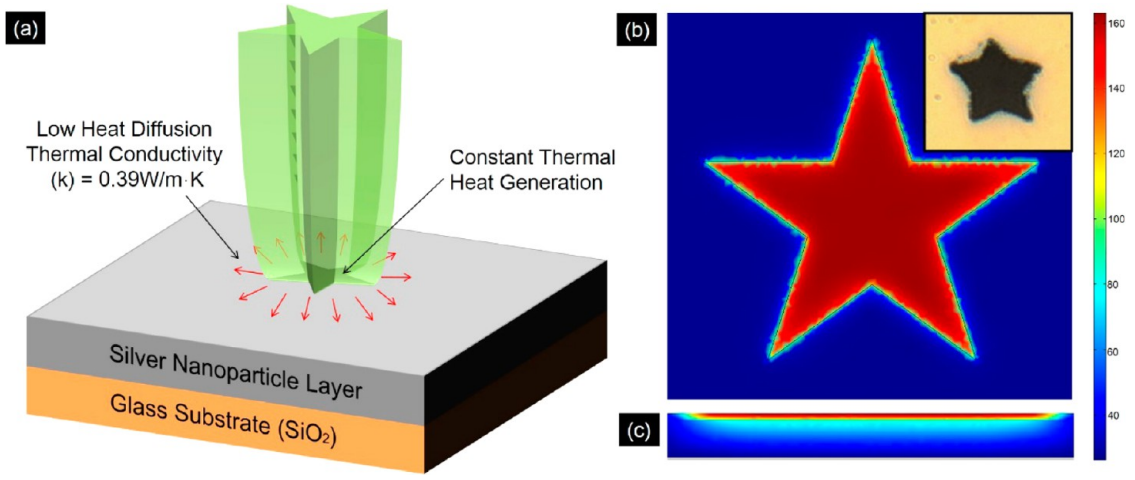

Figure 3. (a) Schematic diagram of photothermal characteristics of laser induced substrate. (b, c) Temperature distribution analyzed by FE analysis.

vigorous stirring for 15 min. 24 mL of pure water with 0.43 M sodium borohydride is rapidly added in organic solution. A reducing reaction is performed for 3 h and 30 min. Excess chloroform in the final product is removed through rotary evaporation. The remnant is cleaned with ethanol and acetone with centrifugation and ultrasonication.

A detailed optical setup of the experiment is shown in Figure 1. Nd:YAG continuous-wave laser at 532 nm wavelength (Millenia V, Spectra Physics) is used for the sintering source. The laser beam passes through a couple of lenses with different focal lengths, and the beam is expanded 5 times to cover a digital micromirror device with 600 × 800 pixels. In this experiment, the total area used from DMD chip is ~1 mm × 1 mm in size to maintain uniform laser power over the whole area. Each mirror of the DMD can be controlled by computer in real time to modulate the projected beam. The modified beam, which is reflected from DMD panel, is focused by a 10× long-working-distance objective lens (Mitutoyo) onto the motorized stage which holds the substrate. Ag NP thin film is first coated on a glass substrate using spin coating. Spin coating is performed with 1500 rpm, and the thickness of the Ag NP layer after the spin coating is measured to be 200 nm. Two charge coupled devices (CCD) are placed at each side of the substrate to focus the DMD modified laser beam onto the substrate while monitoring both sides in real time. After the laser sintering process, unsintered Ag NPs are simply removed by a washing of the substrate with toluene.

3. RESULTS AND DISCUSSIONS

3.1. Thermochemical Characteristics of Ag NPs. The size of Ag NP is measured by TEM, and the substrate for the measurement is fabricated with a self-assembled monolayer of Ag NPs. For the monolayer sample preparation, Ag NPs are diluted with the ethanol and it is dispersed onto a carbon-coated copper grid (FCF300-Cu, Electron Microscopy Sciences). The manufactured sample is observed using TEM equipment (Tecnai G2 F30, FEI company) at an accelerating voltage of 300 kV. The measured sizes of Ag NPs are distributed in a range of 4−6 nm (Figure 2a). TGA and DSC are measured to analyze thermochemical properties of Ag NPs and its thermal sintering behavior. Figure 2b,c shows the graphs of TGA and DSC around 150 °C which are measured by thermal analyzer (SETSYS 16/18) under Argon atmosphere with 10 °C min^{-1}.[12] In both graphs, dramatic changes can be found at ~150 °C. From TGA, weight loss of the Ag NPs is intensified from 150 °C, and this trend can be explained by the evaporation of organic solvents and polymer molecules which covers each Ag NP to sustain the shape of NP and prevent the agglomeration.[12] There is also a striking change at 150 °C of the DSC curve which means that an exothermic reaction or a phase change occurs at ~150 °C. Through these common characteristics, it can be estimated that the melting and the coalescence between Ag NPs occurs at ~150 °C, which is much lower than its bulk melting point as anticipated theoretically from the Gibbs−Thomson equation.

3.2. Finite Element (FE) Simulation for Temperature Estimation. During the laser sintering process, the incoming laser is absorbed by Ag NP film and transformed into the thermal energy, and the resultant temperature distribution is determined by heat generation and the diffusion properties of the Ag NP film itself and the underlying substrate. In the case of Ag NPs at a similar size, the thermal conductivity (0.39 W mK^{-1}) is known to be extremely low, which is 3 orders of magnitude lower than the thermal conductivity of bulk Ag (429 W mK^{-1}).[4] The thermal conductivity of the Ag NP film is significantly poorer than that of its bulk counterpart because of the surfactant that exists as thiol-stabilizer.[19−21] Also, thermal conductivity of a nanostructure is determined by phonon transport through the percolation inside the structure. For the NPs at very small size, the mean free path of the phonon is larger than the size of NP itself, so that the phonon scattering at the interface of the particle contributes significantly[22,23] to the macroscopic thermal conductivity.

The temperature distribution of the laser heated Ag NP layer is simulated with finite element (FE) analysis. Figure 3a shows a schematic diagram of the simulation and thermal characteristics of the layer when the Ag NP layer is heated with a star-shaped laser beam. The FE analysis software to simulate the thermal effects was Comsol Multiphysics with a general heat transfer module. A constant temperature at 300 K is assumed at the outer boundary, while a constant heat flux is applied at the star-shaped area. The lateral area under simulation is 0.1 mm × 0.1 mm, while the thicknesses of the glass substrate and the Ag NP layer is 1 μm and 200 nm, respectively. Due to the low thermal conductivity of the Ag NP layer, the temperature gradient at constant heat generation is very steep, which enables high resolution patterning. Figure 3b shows a diagram with contour lines of equal temperatures whose maximum temperature is similar to the estimated melting temperature of Ag NPs.

3.3. 2D Metal Patterns Fabricated with DMD Modulated Focused Laser Beam. FE simulation is verified through fabricating various shapes of Ag electrode pattern on

dx.doi.org/10.1021/am405323c | ACS Appl. Mater. Interfaces 2014, 6, 2786−2790

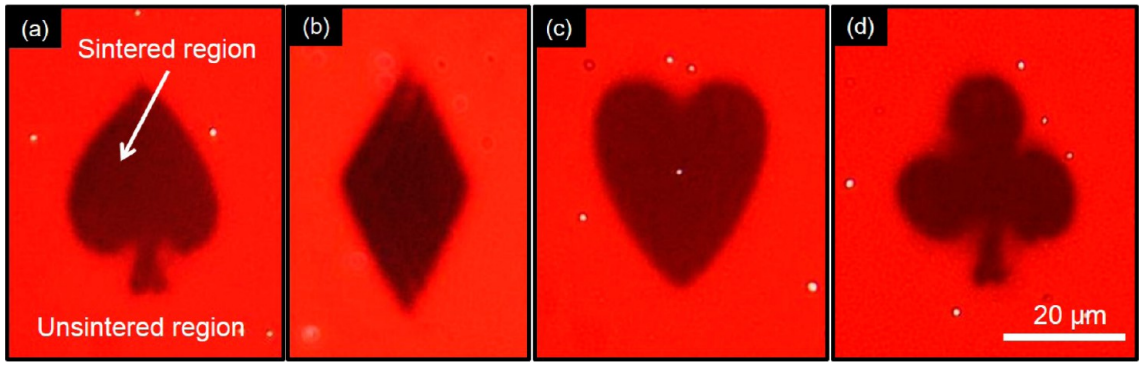

Figure 4. Transmitted microscope images of sintered pattern over glass substrate with various trump shapes. (a) Spade, (b) diamond, (c) heart, and (d) clover.

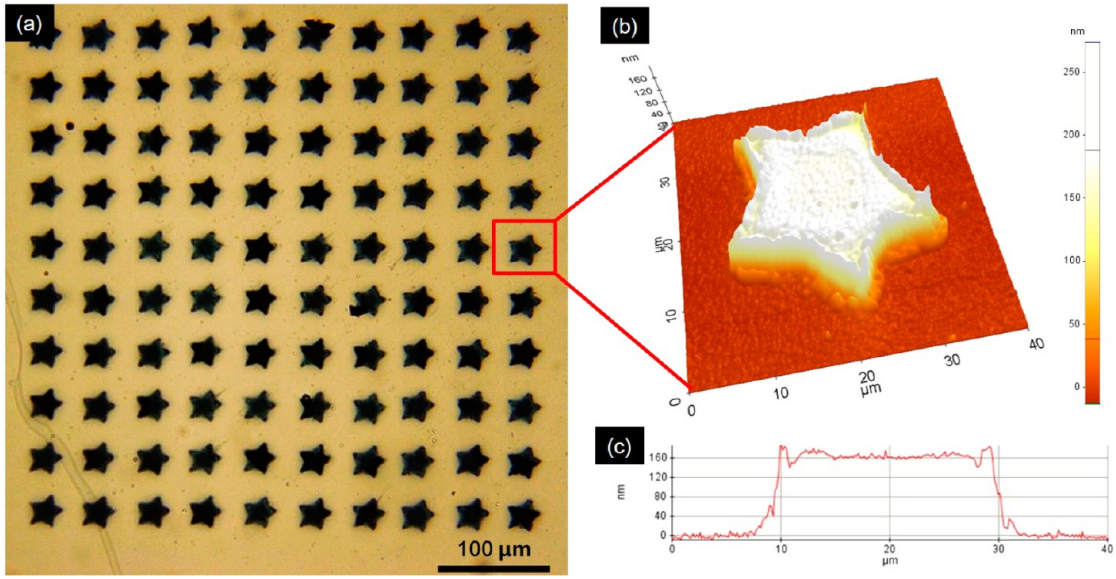

Figure 5. (a) 10 × 10 array of star-shaped pattern array on the 500 μm sized substrate. (b) 3D image of the AFM image of one pattern. (c) Cross sectional view of the AFM image.

the substrate. The sample is prepared on the glass substrate, so that it can be observed by transmitted light microscopy. Various patterns can be obtained by changing the input signals to DMD. Figure 4 shows the transmitted microscope image of the Ag NP ink after the 2D laser sintering of various trump shapes. It can be confirmed from Figure 4 that the transmittance of light is evidently different in the sintered and unsintered region, since the sintered Ag NPs immediately recover its bulk properties and becomes more reflective. From Figure 4, it is verified that the precision of the patterns for the current optical configuration is ~2 μm. The resolution, as well as the overall size of the pattern, can be further controlled by changing the optics. In the current optical setting, the laser exposure is controlled by a mechanical shutter. Its minimum on/off time is ~100 ms and so is the processing time for a single patterning. The characteristic time for a similar laser sintering process was measured to be 5−10 ms in our previous study.[11] Therefore, it is expected that the processing time can be further shortened by using a different scheme such as acousto-optic modulator (AOM) for the laser exposure step. We estimated that the laser power reflected back from DMD can reach ~1 W at maximum, while the objective lens focuses the DMD-modulated laser beam on the area of ~30 μm × 30 μm size. The intensity at the sample is calculated to be ~1.1 × 10^5 W/cm^2, and this is comparable to the previously reported value.[11]

Together with the movement of stage, the metal pattern array can be fabricated on the substrate by step-and-repeat scheme, as confirmed by the 10 × 10 star-shaped silver electrode shown in Figure 5. The size of one star-shape pattern is ~25 μm while the gap is fixed to be 30 μm so that the total area is ~500 μm. Each pattern is fabricated with a single exposure, and a regular metal pattern is continuously fabricated as if DMD modulated focused laser beam is acting as an optical stamp. The uniformity and accuracy of this process on the large area patterning can be confirmed from Figure 5a. The profile of laser sintered 2D metal pattern is further analyzed by atomic force microscopy (AFM). Figure 5b shows a 3D AFM image of a single star-shaped pattern. Its height is about 160 nm, and it shows a very flat surface except at the edge. The rim at the edge of the pattern might be caused by the thermocapillary effect at the early stage of the sintering process. The flat surface and thin thickness of the laser sintered metal pattern has an advantage in the extensive areas of thin film technology.

The electrical resistivity obtained from $I-V$ curve in Figure 6 with laser sintering of Ag NPs is ~10.8 uΩ · cm, which is about 7 times higher than that of bulk silver. The sintering of NPs allows locking between NPs to enhance the overall conductivity

dx.doi.org/10.1021/am405323c | ACS Appl. Mater. Interfaces 2014, 6, 2786−2790

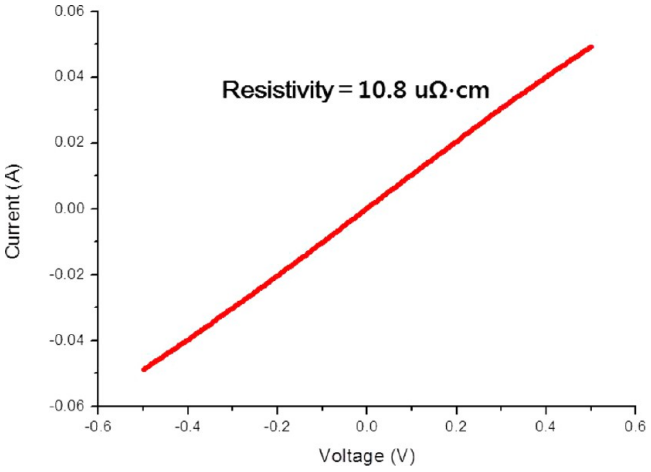

Figure 6. Electrical characteristic of the fabricated silver micropattern.

of the electrode, yet the conductivity is not fully recovered to the bulk one because of electron scattering between the interfaces of the nanopores inside the electrode. Even so, the conductivity of the resultant Ag pattern is low enough to be utilized as an efficient electrode in various applications.

4. CONCLUSIONS

We have demonstrated metal pattern fabrication by 2D laser sintering of Ag NP ink using a DMD modulated focused laser beam. By a simple optical setting with DMD, the beam is modulated to an intended image at the Ag NP ink layer which can be controlled by pixel-addressable input data. The Ag NP layer immediately turns into conductive Ag electrode upon the laser exposure, whereas the resultant Ag pattern shows fine edge sharpness and low electrical resistivity.

The herein proposed selective laser sintering process using DMD successfully eliminated the need of a time-consuming raster scanning procedure for 2D patterns, while including all the advantages of the conventional laser sintering process. This process is also useful for fabricating extensive arrays of thin layered metal patterns, as confirmed by 10 × 10 micro-electrodes produced with uniform size and gap distance through the step-and-repeat scheme.

AUTHOR INFORMATION

Corresponding Authors

*E-mail: maxko@snu.ac.kr. Tel: +82-2-880-7114. Fax: +82-2-880-1513 (S.H.K.).

*E-mail: nakaz79@snu.ac.kr. Tel: +82-2-880-1681. Fax: +82-2-880-1513 (J.Y.).

Author Contributions

¶These authors (Kunsik An and Sukjoon Hong) contributed equally.

Notes

The authors declare no competing financial interest.

ACKNOWLEDGMENTS

This work was supported by National Research Foundation of Korea (NRF) (grant no. 2012-0008779), Global Frontier R&D Program on Center for Multiscale Energy System (grant no. 2012-054172) funded by the Ministry of Science, ICT & Future, and the R&D Convergence Program and ISTK (Korea Research Council for Industrial Science and Technology) (grant no. B551179-10-01-00), and by Seoul National University, Institute of Advanced Machinery and Design (SNU-IAMD).

REFERENCES

(1) Fortunato, E.; Barquinha, P.; Martins, R. *Adv. Mater.* **2012**, *24* (22), 2945−2986.

(2) Ko, S. H.; Pan, H.; Ryu, S. G.; Misra, N.; Grigoropoulos, C. P.; Park, H. K. *Appl. Phys. Lett.* **2008**, *93* (15), 151110.

(3) Zhang, Y.; Feng, H.; Wu, X.; Wang, L.; Zhang, A.; Xia, T.; Dong, H.; Li, X.; Zhnag, L. *Int. J. Hydrogen Energy* **2009**, *34* (11), 4889−4899.

(4) Kim, W.; Zide, J.; Gossard, D.; Klenov, D.; Stemmer, S.; Shakouri, A.; Majumdar, A. *Phys. Rev. Lett.* **2006**, *96* (4), 045901.

(5) Vaezia, M.; Chianrabutra, S.; Mellor, A.; Yang, S. *Virtual Phys. Prototyping* **2013**, *8* (1), 19−50.

(6) Seung, H. K.; Heng, P.; Costas, P. G.; Christine, K. L.; Jean, M. J. F.; Dimos, P. *Nanotechnology* **2007**, *18* (34), 345202.

(7) Smith, P. J.; Shin, D. Y.; Stringer, J. E.; Derby, B.; Reis, N. J. *Mater. Sci.* **2006**, *41* (13), 4153−4158.

(8) Jain, K.; Klosner, M.; Zemel, M.; Raghunandan, S. *Proc. IEEE* **2005**, *93* (8), 1500−1510.

(9) Birnstock, J.; Blassing, J.; Hunze, A.; Scheffel, M.; Stobel, M.; Heuser, K.; Wittmann, G.; Worle, J.; Winnacker, A. *Appl. Phys. Lett.* **2001**, *78* (24), 3905−3907.

(10) Guo, L. J.; Cheng, X.; Chou, C.-F. *Nano Lett.* **2004**, *4* (1), 69−73.

(11) Yeo, J.; Hong, S.; Lee, D.; Hotz, N.; Lee, M.-T.; Grigoropoulos, C. P.; Ko, S. H. *PLoS One* **2012**, *7* (8), No. e42315.

(12) Son, Y.; Yeo, J.; Ha, C. W.; Lee, J.; Hong, S.; Nam, K. H.; Yang, D.-Y.; Ko, S. H. *Thermochim. Acta* **2012**, *542*, 52−56.

(13) Ko, S. H.; Chung, J.; Hotz, N.; Nam, K. H.; Grigoropoulos, C. P. J. *Micromech. Microeng.* **2010**, *20* (12), 125010.

(14) Singh-Gasson, S.; Green, R. D.; Yue, Y.; Nelson, C.; Blattner, F.; Sussman, M. R.; Cerrina, F. *Nat. Biotechnol.* **1999**, *17* (10), 974−978.

(15) Totsu, K.; Esashi, M. *J. Vac. Sci. Technol., B: Microelectron. Nanometer Struct.–Process., Meas., Phenom.* **2005**, *23*, 1487−1490.

(16) Wang, T.; Quaglio, M.; Pirri, F.; Cheng, Y.-C.; Busacker, D.; Cerrina, F. *Proc. SPIE* **2009**, *7274*, 72742O.

(17) Pan, H.; Hwang, D. J.; Ko, S. H.; Clem, T. A.; Fréchet, J. M. J.; Bäuerle, D.; Grigoropoulos, C. P. *Small* **2010**, *6* (16), 1812−1821.

(18) Korgel, B. A.; Fitzmaurice, D. *Adv. Mater.* **1998**, *10* (9), 661−665.

(19) Wang, R.; Segalman, R.; Majumdar, A. Thermal Conductance of Au-octanedithiol-GaAs Junctions. *International heat transfer conference 13*; Begell House Publishers: Redding, Connecticut, 2006.

(20) Shalkevich, N.; Escher, W.; Bürgi, T.; Michel, B.; Si-Ahmed, L.; Poulikakos, D. *Langmuir* **2010**, *26* (2), 663−670.

(21) Johnson, S. R.; Evans, S. D.; Brydson, R. *Langmuir* **1998**, *14* (23), 6639−6647.

(22) Venkatasubramanian, R. *Phys. Rev. B: Condens. Matter Mater. Phys.* **2000**, *61* (4), 3091−3097.

(23) Borca-Tasciuc, T.; Liu, W.; Liu, J.; Zeng, T.; Song, D. W.; Moore, C. D.; Chen, G.; Wang, K. L.; Goorsky, M. S.; Radetic, T.; Gronsky, R.; Koga, T.; Dresselhaus, M. S. *Superlattices Microstruct.* **2000**, *28* (3), 199−206.